Surface Tension and the Strain-Dependent Topography of Soft Solids

Nicolas Bain, Anand Jagota, Katrina Smith-Mannschott, Stefanie Heyden, Robert Style, Eric Dufresne

Surface Tension and the Strain-Dependent Topography of Soft Solids

Nicolas Bain,[1,*] Anand Jagota,[2,†] Katrina Smith-Mannschott,[1] Stefanie Heyden,[1]
Robert W. Style,[1] and Eric R. Dufresne[1,‡]
[1]Department of Materials, ETH Zürich, 8093 Zürich, Switzerland
[2]Departments of Bioengineering, and of Chemical and Biomolecular Engineering, Lehigh University, Bethlehem, Pennsylvania 18017, USA

(Received 28 April 2021; revised 23 August 2021; accepted 30 September 2021; published 8 November 2021)

When stretched in one direction, most solids shrink in the transverse directions. In soft silicone gels, however, we observe that small-scale topographical features grow upon stretching. A quantitative analysis of the topography shows that this counterintuitive response is nearly linear, allowing us to tackle it through a small-strain analysis. We find that the surprising increase of small-scale topography with stretch is due to a delicate interplay of the bulk and surface responses to strain. Specifically, we find that surface tension changes as the material is deformed. This response is expected on general grounds for solid materials, but challenges the standard description of gel and elastomer surfaces.

DOI: 10.1103/PhysRevLett.127.208001

Surface tension is the driving force of a plethora of small-scale phenomena. In liquids, it is responsible for the spherical shape of small drops and for the shape of menisci [1]. In soft solids, surface tension rounds off sharp features [2–5] and more generally governs mechanical responses at small scales [6–14]. Despite the growing interest in soft solids for applications in microsystems and robotics [15–17], the essential nature of their surface properties remains elusive.

Generally, soft solids come in two forms, elastomers and gels. Elastomers are made by lightly cross-linking a polymeric liquid. Gels are cross-linked networks swollen with a liquid solvent. In both cases, it is generally assumed that molecules can seamlessly rearrange at the surface, resulting in liquidlike surface properties. Specifically, it is expected that the surface tension is independent of the applied strain. Recently, this assumption has been tested with wetting experiments. Macroscopic experiments [18] found no evidence for strain-dependent surface energy in elastomers. However, microscopic experiments with gels [19,20] found a marked increase of surface tension with applied strain, a characteristic feature of solid surfaces [21–23]. While recent theoretical works have validated the microscopic method [24,25], others have called it into question because of the singular nature of the three-phase contact line [26]. Therefore, there is an urgent need for measurements of the strain dependence of surface tension in soft solids that do not rely on wetting phenomena.

Here, we examine the strain dependence of surface tension for a family of silicone solids, by quantifying their surface topography as a function of applied stretch. For the softest silicone gels, we observe a counterintuitive increase of the amplitude of surface topography. A small-strain analysis of this increase shows that it can only be quantitatively captured by a balance of strain-stiffening bulk properties and solidlike surface tension.

We cure polydimethylsiloxane (PDMS) gels inside dog-bone shaped poly(methyl methacrylate) molds, so that the central section of the dog bone has a 3×2 mm^2 cross section and length of 20 mm, Fig. 1(a). A periodic

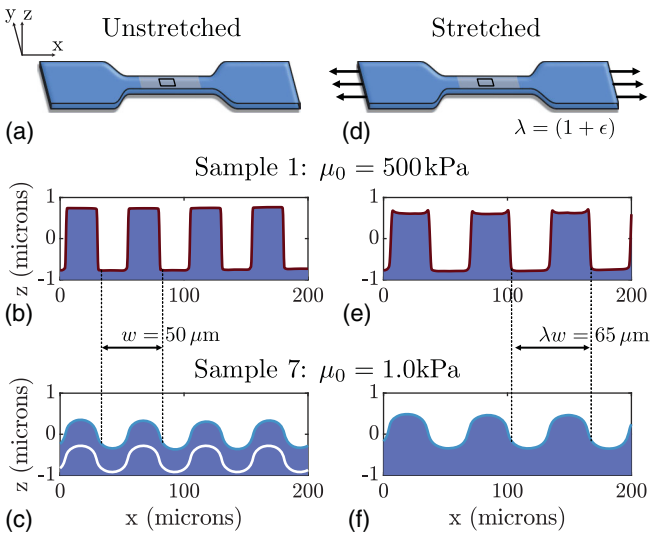

FIG. 1. Experimental overview. (a) Schematic of the patterned dog-bone samples. (b) and (c) Averaged unstretched surface profile for the stiffest gel, Sample 1, and for the softest gel, Sample 7, respectively. The white line in (c) corresponds to the profile prediction from the linear flattening model, Eq. (1), applied to all Fourier modes of the initial profile (b), with shear modulus $\mu_0 = 1.0$ kPa and surface tension $\Upsilon_0 = 25.3$ mN/m, Table I. It agrees perfectly with the experimental profile and has been shifted down to be visible. In (d), the stretch λ and the strain ϵ are calculated from the change of the pattern wavelength. (e),(f) Averaged surface profile for the stiffest and for the softest gel, respectively, stretched by 30%.

rectangular grating of wavelength 50 μm and amplitude 1.52 ± 0.01 μm is applied to the surface during curing, to give the profile shown in Fig. 1(b). The grating is made of low-surface-tension chemically inert fluoroplastic (3M DyneonTM Fluoroplastic Granules THV 500GZ) by melting fluoroplastic beads at 200 °C for 8 h onto a stiff PDMS grating [27]. Samples are cured against the fluoroplastic mold at 40 °C for over a week to ensure full cross-linking after detachment from the grating; the patterned surface on the PDMS sample relaxes to a new shape, in which surface stresses and bulk elastic stresses balance [2,3,28], Fig. 1(c). We then stretch the dog-bone shaped sample, Fig. 1(d), and measure the surface topography at each stretch state with a 3D optical profiler (S-neox, Sensoscan, 40× objective). The surface topography relaxes completely within a few minutes. We image only the middle of the sample where we expect uniform stretching conditions. We conduct the experiment on seven silicone samples with different stiffnesses, each measured independently with an indentation test. For each sample, all measurements are at roughly the same location. We name them "Sample 1" to "Sample 7" in order of decreasing stiffness (see Table I for properties and Supplement Sec. 1 [29] for experimental details).

To develop a qualitative understanding of the results, we first contrast the surface profiles of the stiffest and softest samples, Fig. 1. Surface profiles for the other gels are provided in Supplement Sec. 1.3 [29]. Each profile is an average of one topography measurement along the transverse direction y. Unstretched, the stiffer sample nicely reproduces the topography of the initial mold, Fig. 1(b). This is the behavior we expect from a stiff solid, which is stiff enough to resist significant deformation by surface tension. Conversely, the topography of the softer gel strongly deviates from the one of the initial mold. The peak-to-peak amplitude is halved, and the shape is significantly rounded-off, Fig. 1(c).

To explain this behavior, we begin with a force balance at the solid-air interface of an *unstretched* solid. Akin to the experiments, we consider a solid with an undulating surface, periodic in the x direction and invariant along the y direction, Fig. 1. For simplicity we assume the initial surface profile to be sinusoidal, $h_0 \cos qx$, where $q = 2\pi/w$ is the pattern's wave vector and h_0 the surface amplitude when the sample is attached to the mold. When released from the mold, the surface deforms into its new equilibrium profile $h_f \cos qx$. We estimate the final amplitude h_f by balancing the vertical stresses on both sides of the solid-air interface. On the bulk side, the normal displacement of the surface $v = (h_f - h_0)\cos qx$ creates a normal stress response σ_z. For an isotropic incompressible linear elastic solid, this stress is proportional to the shear modulus μ_0: $\sigma_z = 2\mu_0|q|v$ [33]. On the other hand, surface tension Υ_0 creates a jump in the stresses across the undulating interface, σ_Υ, proportional to the local curvature of the final profile: $\sigma_\Upsilon = -q^2\Upsilon_0 h_f \cos qx$ [6]. The solid is at mechanical equilibrium when the jump in stresses caused by surface tension is equal to the stress response from the bulk deformation $\sigma_\Upsilon = \sigma_z$. From this stress balance we express the final amplitude as a function of the initial one,

$$h_f = \frac{h_0}{1 + |q|\frac{\Upsilon_0}{2\mu_0}}, \tag{1}$$

which we call the flattening equation [2,3,28]. Assuming linear response, this process can be applied to any Fourier mode of a nonsinusoidal surface. Simply stated, surface tension acts as a low-pass filter with a cut-off length equal to the elastocapillary length $\Upsilon_0/2\mu_0$.

We use this result to determine the surface tension of the soft gels (3–7) by inverting the flattening equation Eq. (1) for the first Fourier mode of the unstretched samples. For all the soft gels we obtain nearly the same unstretched surface tension, $\Upsilon_0 = 25.7 \pm 2.1$ mN/m, Table I. This value is close to $\gamma = 21 \pm 1$ mN/m, the surface tension of uncross-linked PDMS [34]. To further validate this model, we apply the flattening equation to each of the Fourier modes of the mold for the softest sample, and nicely recover the experimental profile, as shown by the light curve in Fig. 1(c).

We now return to the qualitative comparison of the softest and stiffest samples, and consider the effect of stretching on their surface profiles, Figs. 1(e) and 1(f). With stretch, the wavelength of both surface profiles increases.

TABLE I. Summary table for the properties of measured when unstretched. We measure the shear modulus μ_0 from an independent indentation test, and the first Fourier mode $\tilde{h}_1$ from the surface topography. We measure the surface tension Υ_0 from the linear flattening theory Eq. (1), using $h_0 = 0.97 \pm 0.01$ μm for reference, measured from the initial molds.

Name	Industrial supplier	Shear modulus μ_0	First mode $\tilde{h}_1$	Surface tension Υ_0
Sample 1	Sylgard184, Dow Corning Toray	500 ± 10 kPa	$0.96 \pm .01$ μm	···
Sample 2	Sylgard184, Dow Corning Toray	500 ± 10 kPa	$0.97 \pm .01$ μm	···
Sample 3	DMS-V31/HMS-301 Gelest	3.9 ± 0.1 kPa	$0.68 \pm .01$ μm	26.3 ± 0.7 mN/m
Sample 4	CY52-276, Dow Corning Toray	2.0 ± 0.2 kPa	$0.56 \pm .01$ μm	27.2 ± 1.2 mN/m
Sample 5	CY52-276, Dow Corning Toray	1.9 ± 0.1 kPa	$0.52 \pm .01$ μm	21.8 ± 1.1 mN/m
Sample 6	CY52-276, Dow Corning Toray	1.9 ± 0.1 kPa	$0.50 \pm .01$ μm	27.9 ± 0.4 mN/m
Sample 7	DMS-V31/HMS-301 Gelest	1.0 ± 0.1 kPa	$0.38 \pm .01$ μm	25.3 ± 1.9 mN/m

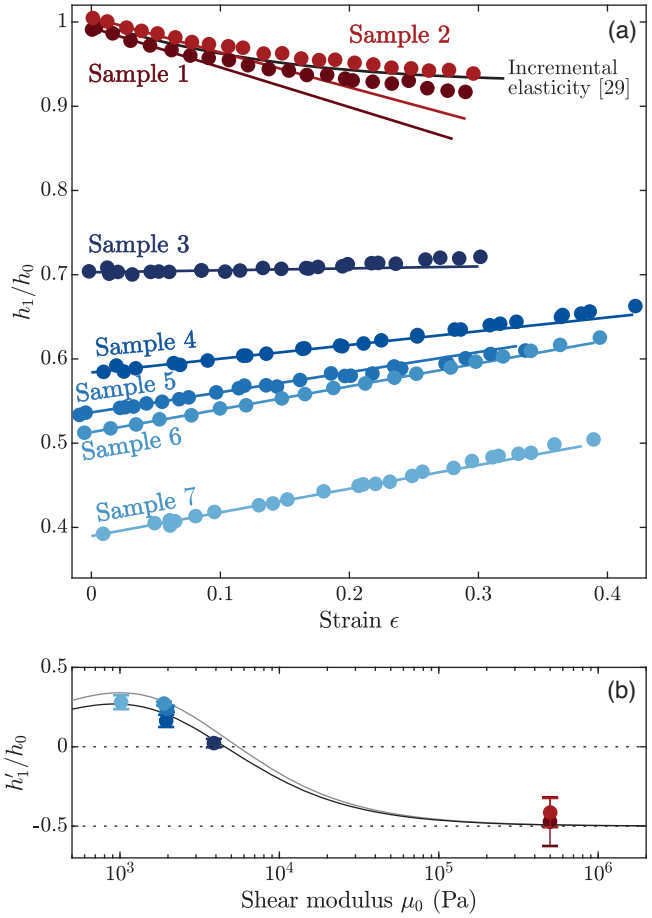

FIG. 2. Quantification of the strain-dependent topography. (a) Strain-dependent amplitude of the first Fourier mode amplitude, h_1/h_0, for all samples as a function of strain, ϵ. Circles: experimental data. Error bars are smaller than marker size. Solid colored lines: linear fits of the data at small strains, for up to 15% for samples (3–7) and up to 5% for samples (1–2). Black line: prediction from incremental elasticity (see Supplement Sec. 2.4 [29]). (b) Initial slope, h_1'/h_0, of the strain-dependent first Fourier mode, as measured in (a), for all samples as a function of shear modulus, μ_0. Error bars correspond to the 95% confidence interval of the linear fit. Gray line: prediction of the initial slope from linear expansion Eq. (3) no surface elasticity $s = 0$. Black line: prediction of the initial slope from linear expansion Eq. (3) with surface elasticity $s = 0.3$. These two predictions were made for $\alpha = 1/2$ and $b = 5/4$.

The peak-to-peak amplitude of the stiffest gel goes down, as expected due to its near incompressibility, Fig. 1(e). Surprisingly, the peak-to-peak amplitude of the softest gel *increases*, even though it is also nearly incompressible, Fig. 1(f).

To quantify the strain-dependent topography of stiff and soft gels, we Fourier decompose the surface profile at each stretched state. We measure the strain, ϵ, from the difference between the wavelength of the periodic grating at each stretch state and the initial wavelength of 50 μm, Fig. 1. The amplitude of the first Fourier mode for all seven gels, $\tilde{h}_1$, are shown in Fig. 2(a). Each measurement is repeated six times to suppress contributions from environmental noise. While the amplitude of the first mode decreases monotonically with stretch for the MPa-scale elastomers, the amplitude of the first mode exhibits the unexpected increase with applied stretch for all the kPa-scale gels.

The response of the first Fourier mode amplitude to stretch is surprisingly linear, especially for the softer samples, Fig. 2(a). Therefore, we quantify the stretch response with the initial slope $h_1' = dh_1/d\epsilon$ from a linear fit at small strains, up to 15% for the kPa samples and up to 5% for the MPa samples, Fig. 2(b). The slope decreases from a positive value for the softest samples to a negative value for the stiffest one, crossing zero at a shear modulus around 5 kPa.

To elucidate these counterintuitive observations, we investigate the competition of surface tension and bulk elasticity during stretching. If we assume the flattening process to be linear, we can apply it as a perturbation to a stretched solid initially devoid of surface tension. Within this assumption, stretching the solid accounts to changing Eq. (1) in four ways. First, the initial surface amplitude h_0 is replaced by its stretched counterpart $h_\epsilon(\epsilon)$. Then the period of the surface profile lengthens with strain, and the associated wave vector becomes $q/(1+\epsilon)$. If solidlike, the value of the surface tension will also be strain dependent $\Upsilon_\epsilon(\epsilon)$. Finally, the bulk elastic properties are also subject to change, responding to a sinusoidal vertical displacement with a strain-dependent effective shear modulus $\mu_\epsilon(\epsilon)$. In short, all the terms of the flattening equation Eq. (1) become strain dependent,

$$h_f(\epsilon) = \frac{h_\epsilon}{1 + |\frac{q}{(1+\epsilon)}|\frac{\Upsilon_\epsilon}{2\mu_\epsilon}}. \tag{2}$$

We now conduct a linear expansion around small strains, $\epsilon \ll 1$. At first order, the final amplitude is linear in strain $h_f(\epsilon) = h_f(0) + h_f'\epsilon + \mathcal{O}(\epsilon^2)$, with unstrained amplitude, $h_f(0)$, and initial slope, h_f', measured in Fig. 2(b). Linearizing each term of the strain-dependent flattening equation (2), $h_\epsilon = h_0(1-\alpha\epsilon) + \mathcal{O}(\epsilon^2)$, $\mu_\epsilon = \mu_0(1 + b\epsilon) + \mathcal{O}(\epsilon^2)$ and $\Upsilon_\epsilon = \Upsilon_0(1 + s\epsilon) + \mathcal{O}(\epsilon^2)$, we find their respective contributions to the initial slope

$$h_f' = h_0 \frac{(|q|\frac{\Upsilon_0}{2\mu_0}[1 - \alpha + b - s] - \alpha)}{(1 + |q|\frac{\Upsilon_0}{2\mu_0})^2}. \tag{3}$$

In the limit where the bulk and surface properties are strain independent (i.e., $s = b = 0$), we see that positive initial slopes are only possible when surface tension is sufficient to overwhelm the impact of the bulk-term, α. The parameter α characterizes the strain-dependent amplitude of a patterned solid in the absence of surface tension. In the geometry of the present experiment, imposing a longitudinal strain to a slender beam, incompressibility requires

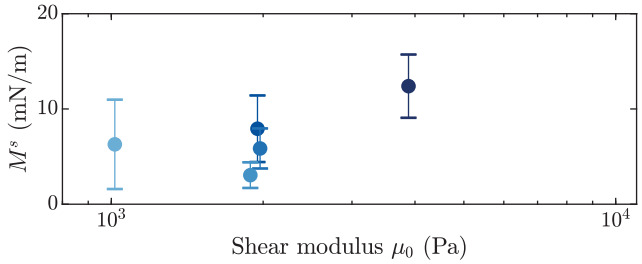

FIG. 3. Surface and bulk elastic constants. Surface longitudinal modulus, M^s, as a function of shear modulus μ_0 for all four soft samples. The error bars correspond to the 95% confidence interval of the linear fits in Fig. 2.

$\alpha = 1/2$, which is in good agreement with the initial slope of the MPa samples, Fig. 2(b). When the materials' properties depend on the strain (i.e., $s, b \neq 0$), contributions from the surface and bulk have opposing effects: while the bulk strain-stiffening ratio b increases the slope, surface elasticity ratio s decreases it.

To isolate the effect of surface elasticity, we must first evaluate the strain-dependent response of the bulk. To do so, we need to identify the appropriate nonlinear constitutive relation for our materials. As shown in the Supplement Sec. 1.2 [29], our silicone based materials are well modeled as incompressible Neo-Hookean solids over the current range of strains. In our experimental geometry, incremental elasticity [35] gives a small-strain stiffening ratio of $b = 5/4$, as derived in Supplement Sec. 2 [29]. The validity of the incremental elasticity model is verified numerically in Supplement Sec. 3 [29]. This result accurately predicts the strain-dependent topography of the MPa samples [Fig. 2(a)].

With this, we can now investigate the role of surface elasticity. We plot predicted values of h'_f/h_0 versus shear modulus in Fig. 2(b). While liquidlike surface tension systematically overestimates the initial slope (gray curve, $s = 0$), we find better agreement between theory and experiment for $s = 0.3$. This systematic overshoot is very explicit in Supplement Sec. 3, where we compare the experimental strain-dependent topography with the analytical and numerical models. Physically, we can interpret nonzero s values as surface elasticity, with an elastic constant $M^s = s\Upsilon_0$. We can independently determine the value of M^s from the measured values of h'_f in each experiment, using Eq. (3). The resulting values of M^s are plotted for all the soft samples in Fig. 3. Similar to [19,20], we find a nonzero surface modulus for all the soft gels. However, we find a weaker effect of surface elasticity. In this experiment, we find $M^s \approx 10$ mN/m, with significant variability across nominally identical samples. According to the wetting measurements of [20,25], we would expect $M^s = 52$ mN/m, see Supplement Sec. 4 [29]. We show in Supplement Sec. 1.4 that this result is independent of the pattern wavelength.

We have found that the strain-dependent topography of soft silicone gels is consistent with nonzero surface elastic constants. We observe notable variability in the surface elastic moduli of nominally identical samples. The factors underlying this sample-to-sample variation demand further investigation. Qualitatively, we reach the same conclusions as previous wetting experiments [19,20]. Quantitatively, we find significantly smaller surface elastic moduli. This discrepancy could arise from nonlinear stress focusing at sharp wetting ridges [24,26], or differences in surface preparation [36]. While both experiments couple surface elasticity and bulk nonlinearities, the singular behavior of a three-phase contact line complicates their decoupling [24,26]. The present experiment avoids this singularity, allowing us to develop a simple framework to disentangle bulk and surface effects. More generally, our experiments suggest that the surface mechanical properties of swollen polymer networks can have significant contributions from both their solvent and network. They raise basic questions in physics of polymer networks that have received limited theoretical attention. How is the structure of the polymer network different at the surface than in the bulk? What sets the magnitude of surface elastic moduli? Can they be tuned independently of bulk elastic moduli? Can we engineer surface elastic constants by curing in different environments, or through the addition of surface-active species, as done with liquid-liquid interfaces [37–39]? We hope that the answers to these questions will provide fresh insights into the physics of soft solids, and enable future applications in wetting and adhesion.

We acknowledge support from ETH Zürich Postdoctoral Fellowship. We thank J. Snoeijer, J. Dervaux, and T. Salez for insightful discussions. We also thank the Isa Lab, as well as O. Dudaryeva for introducing us to the use of fluoroplastic to pattern silicone surfaces.

*nicolas.bain@mat.ethz.ch
†anj6@lehigh.edu
‡eric.dufresne@mat.ethz.ch

[1] P.-G. De Gennes, F. Brochard-Wyart, and D. Quéré, *Capillarity and Wetting Phenomena: Drops, Bubbles, Pearls, Waves* (Springer Science & Business Media, New York, 2013).
[2] N. Lapinski, Z. Liu, S. Yang, C.-Y. Hui, and A. Jagota, Soft Matter **15**, 3817 (2019).
[3] D. Paretkar, X. Xu, C.-Y. Hui, and A. Jagota, Soft Matter **10**, 4084 (2014).
[4] A. Jagota, D. Paretkar, and A. Ghatak, Phys. Rev. E **85**, 051602 (2012).
[5] S. Mora, C. Maurini, T. Phou, J.-M. Fromental, B. Audoly, and Y. Pomeau, Phys. Rev. Lett. **111**, 114301 (2013).
[6] R. W. Style, A. Jagota, C.-Y. Hui, and E. R. Dufresne, Annu. Rev. Condens. Matter Phys. **8**, 99 (2017).
[7] B. Andreotti and J. H. Snoeijer, Annu. Rev. Fluid Mech. **52**, 285 (2020).

[8] S. Mora, T. Phou, J.-M. Fromental, L. M. Pismen, and Y. Pomeau, Phys. Rev. Lett. **105**, 214301 (2010).
[9] E. R. Jerison, Y. Xu, L. A. Wilen, and E. R. Dufresne, Phys. Rev. Lett. **106**, 186103 (2011).
[10] R. W. Style, C. Hyland, R. Boltyanskiy, J. S. Wettlaufer, and E. R. Dufresne, Nat. Commun. **4**, 2728 (2013).
[11] R. W. Style, R. Boltyanskiy, Y. Che, J. S. Wettlaufer, L. A. Wilen, and E. R. Dufresne, Phys. Rev. Lett. **110**, 066103 (2013).
[12] S. J. Park, B. M. Weon, J. San Lee, J. Lee, J. Kim, and J. H. Je, Nat. Commun. **5**, 4369 (2014).
[13] K. E. Jensen, R. Sarfati, R. W. Style, R. Boltyanskiy, A. Chakrabarti, M. K. Chaudhury, and E. R. Dufresne, Proc. Natl. Acad. Sci. U.S.A. **112**, 14490 (2015).
[14] C. W. Barney, C. E. Dougan, K. R. McLeod, A. Kazemi-Moridani, Y. Zheng, Z. Ye, S. Tiwari, I. Sacligil, R. A. Riggleman, S. Cai *et al.*, Proc. Natl. Acad. Sci. U.S.A. **117**, 9157 (2020).
[15] D. Huh, B. D. Matthews, A. Mammoto, M. Montoya-Zavala, H. Y. Hsin, and D. E. Ingber, Science **328**, 1662 (2010).
[16] S. P. Lacour, G. Courtine, and J. Guck, Nat. Rev. Mater. **1**, 16063 (2016).
[17] S. Kim, C. Laschi, and B. Trimmer, Trends Biotechnol. **31**, 287 (2013).
[18] R. D. Schulman, M. Trejo, T. Salez, E. Raphaël, and K. Dalnoki-Veress, Nat. Commun. **9**, 982 (2018).
[19] Q. Xu, K. E. Jensen, R. Boltyanskiy, R. Sarfati, R. W. Style, and E. R. Dufresne, Nat. Commun. **8**, 555 (2017).
[20] Q. Xu, R. W. Style, and E. R. Dufresne, Soft Matter **14**, 916 (2018).
[21] R. Shuttleworth, Proc. Phys. Soc. London Sect. A **63**, 444 (1950).
[22] M. E. Gurtin and A. I. Murdoch, Arch. Ration. Mech. Anal. **57**, 291 (1975).
[23] W. Haiss, Rep. Prog. Phys. **64**, 591 (2001).
[24] A. Pandey, B. Andreotti, S. Karpitschka, G. J. van Zwieten, E. H. van Brummelen, and J. H. Snoeijer, Phys. Rev. X **10**, 031067 (2020).
[25] S. Heyden, N. Bain, Q. Xu, R. W. Style, and E. R. Dufresne, Proc. R. Soc. A **477**, 20200673 (2021).
[26] R. Masurel, M. Roché, L. Limat, I. Ionescu, and J. Dervaux, Phys. Rev. Lett. **122**, 248004 (2019).
[27] S. Begolo, G. Colas, J.-L. Viovy, and L. Malaquin, Lab Chip **11**, 508 (2011).
[28] C.-Y. Hui, Z. Liu, N. Bain, A. Jagota, E. R. Dufresne, R. W. Style, R. Kiyama, and J. P. Gong, Proc. R. Soc. A **476**, 20200477 (2020).
[29] See Supplemental Material at http://link.aps.org/supplemental/10.1103/PhysRevLett.127.208001 for further details on the experiments, derivation and validation of the incremental elasticity model, which includes Refs. [30–32].
[30] Y. Lin and C.-Y. Hui, and H. Conway, J. Polym. Sci., Part B: Polym. Phys. **38**, 2769 (2000).
[31] H. Gao, J. Mech. Phys. Solids **39**, 443 (1991).
[32] S. T. Milner, J. Joanny, and P. Pincus, Europhys. Lett. **9**, 495 (1989).
[33] K. L. Johnson, *Contact Mechanics* (Cambridge University Press, Cambridge, England, 1987).
[34] V. Bergeron and D. Langevin, Phys. Rev. Lett. **76**, 3152 (1996).
[35] M. A. Biot, *Mechanics of Incremental Deformations* (John Wiley & Sons, Inc., New York, 1965).
[36] In the wetting experiments, silicone was cured in air. Here, silicone was cured against a teflon surface and removed by peeling.
[37] L. Champougny, B. Scheid, F. Restagno, J. Vermant, and E. Rio, Soft Matter **11**, 2758 (2015).
[38] M. Pepicelli, T. Verwijlen, T. A. Tervoort, and J. Vermant, Soft Matter **13**, 5977 (2017).
[39] G. G. Fuller and J. Vermant, Annu. Rev. Chem. Biomol. Eng. **3**, 519 (2012).